Ultrasonic welding of lap joints of PEI plates with PEI/CF-fabric prepregs

V.O. Alexenko, S.V. Panin, S.A. Bochkareva
Institute of Strength Physics and Materials Science SB RAS, Tomsk, Russia
vl.aleksenko@mail.ru, http://orcid.org/0000-0003-4375-9132
svp@ispms.ru, http://orcid.org/0000-0001-7623-7360
svetlanab7@yandex.ru, http://orcid.org/0000-0003-4889-6128

Tian Defang
National Research Tomsk Polytechnic University, Tomsk, Russia
Defan1@tpu.ru, http://orcid.org/0000-0001-2345-6789

I.L. Panov
National Research Tomsk State University, Tomsk, Russia
panov.iliya@mail.ru, http://orcid.org/0000-0003-2321-7109

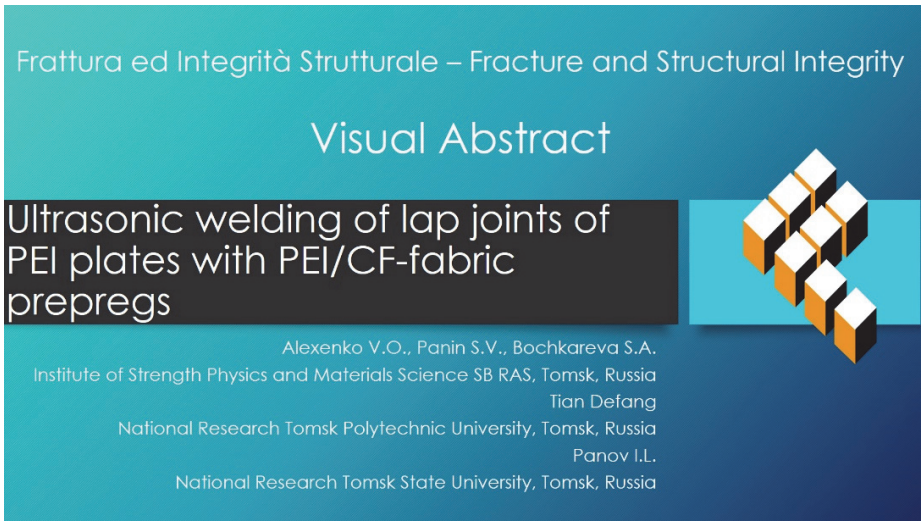

Citation: Alexenko V.O., Panin S.V., Bochkareva S.A., Defang, T., Panov, I.L., Ultrasonic welding of lap joints of PEI plates with PEI/CF-fabric prepregs, Frattura ed Integrità Strutturale, 68 (2024) 390-409.

Received: 30.01.2024
Accepted: 13.03.2024
Published: 15.03.2024
Issue: 04.2024

KEYWORDS. Ultrasonic welding; Lap joint; Polyetherimide; Carbon fiber; Prepreg.

INTRODUCTION

Ultrasonic welding (USW) is one of the most common techniques for joining parts from different thermoplastics [1]. In addition, it can be applied for manufacturing layered composites (laminates) based on high-temperature binders reinforced with high-strength fibers (or fabrics) [2,3]. In this way, a consumable film, the so-called energy

director (ED), is placed between the parts to be welded for minimizing their damage in the fusion zone. As a result, such procedures become, in general, similar to the soldering (or brazing) process. Typically, materials that are easily fusible than the thermoplastic binders are used as EDs. In some cases, they are perforated or fabricated as meshes (by 3D printing for example) [4].

Liu et al. have shown that use of triangular shaped ED is beneficial for USW of neat polypropylene (PP) with polypropylene loaded with 10% fiberglass; however, semicircular EDs provide better quality when composites with a higher fiber content were welded [5]. Villegas, I.F. [6] studied the influence of various configurations, orientations and shapes of EDs on the quality of US-welded lap joints. Carbon fiber reinforced PEI composites were experimentally investigated. The lap-joints were compared over layer shear strength (LSS) under static tension tests. It has been found that the orientation of ED did not significantly affect the value of LSS. At the same time, the adhesion strength of laminates with multiple ED were increased with enlarging ED thickness up to a certain threshold. Conversely, a subsequent increase in the thickness of the ED gave rise to decreasing the LSS value by 34%

Xiaolin Wang [7] discussed the effect of the ED dimension and the apex angle upon the heating process at USW. The simulation results have shown that the apex angle exerted a more significant effect on the heating rate in contrast to the thickness of EDs. In addition, the apex angle strongly affects the temperature distribution in EDs. It was shown that the ED's apex angle of 90 ° and the cross-sectional area ~0.25 mm^2 were best suited for the USW of CF/PEEK laminates.

Suresh et al. [5] have found out that application of triangular shaped ED at the USW are responsible for higher temperatures at the interface as compared to semicircular EDs. The former concentrated more thermal energy (due to the smaller area) that resulted in faster melting and higher tensile strength. On contrary, Goto et al. [8] estimated the shear and tensile strength of cross-ply and twill woven joints of polyamide laminate reinforced with carbon fiber. In doing so, flat ED (made of neat polymer) was utilized. Their results are consistent with experimental studies conducted by Villegas et al. [9]. The heating rate was about twice as high for the carbon fiber reinforced PPS lap joints. However, the shear strength for lap joints with triangular shaped EDs was only slightly higher as compared US-with one welded using flat EDs.

However, the application of USW is rarely described as an industrial method for manufacturing fiber-reinforced laminates from prepregs based on the thermoplastic binders [10, 11].

The USW assisted fabrication of laminates is an actual issue nowadays. It is caused by several reasons, including: a) non-stationary development of the process in time associated with the non-linear heating of the components being joined [12–14] (in contrast to molding in stacks); b) one-sided input of acoustic energy, converted into frictional heating of the fusion zone [15–17]; c) simultaneous development of the structure formation processes at several interfaces [18, 19]; d) significant differences in the elastic properties of the laminate components, including those affecting the propagation pattern of ultrasonic vibrations [20], etc. One of the efficient options for solving this issue is the use of prepregs based on reinforcing fibers (or fabrics) and the thermoplastic binders [21], as noted above. In addition, the USW parameters have to be optimized for minimizing damage to the prepreg upon the consolidation of components.

In this study, as a model approximation, the authors have investigated USW joints, consisting of two plates (adherends) of high performance plastic polyetherimide (PEI). Prepregs made of a fabric from carbon fibers (CFs) impregnated with PEI were placed between them without any ED, in contrast to previously reported results [22]. To compensate for the lack of the polymer in the fusion zone, binder contents were varied in the prepregs. In addition, the effect of the USW parameters on the structure and the mechanical properties of the joints was analyzed. The main goal of their optimization was the formation of USW joints, characterized by improved functional characteristics.

The paper is structured as follows. Section 2 describes both studied materials and experimental procedures. In Section 3, the results of the investigations of the structure and the mechanical properties of the USW joints are reported for various combinations of the process parameters. Section 4 includes both the methodology and the results of computer simulation, based on the finite element method (FEM), of the deformation behavior of 3D models of the USW joints with different adhesion levels. Section 5 is devoted to the optimization of the USW parameters using the response surface methodology (RSM) approach. In Section 6, preceding conclusions, the obtained results are discussed in detail.

MATERIALS AND EXPERIMENTAL PROCEDURES

For the fabrication of PEI plates (adherends) with dimensions of 100×20×2 mm, a powder (Solver PEI ROOH, China) was used, characterized by an average particle size of 20 μm and a melting point of 260 °C. In this way, an 'RR/TSMP' plunger injection molding machine (Ray-Ran Test Equipment Ltd., Nuneaton, UK) was employed. A mold was heated up to 200–205 °C, while the powder feeder temperature was 370 °C.

Prepregs were manufactured as follows. In order to remove the technological (epoxy) sizing agent from the surface, a CF-fabric was annealed at a temperature of 500 °C for 30 minutes [23]. For impregnation, it was placed in a solution of the PEI powder in N-methylpyrralidone (C_5H_9NO). After that, the solvent was evaporated in an oven (Memmert UN 30, Memmert GmbH, Germany) at a temperature of 170 °C for 6 hours. The final thickness of the impregnated CF-fabric was ~500 μm. Then, it was subjected to compressing molding order to vary both the binder contents in the prepregs and their thickness. As a result, the PEI/CF-fabric ratios in the prepregs were 23/77, 30/70 and 43/57 wt. %. Since these ratios were varied by changing the compressing molding durations, their thicknesses were 260, 300 and 360 μm, respectively. At the minimum PEI content, the prepreg thickness was comparable to that for the initial CF-fabric (~230–250 μm).

Based on the previous research results [24] and some trial tests, the following USW parameters were applied: clamping pressure (P) of 1.7 atm; USW durations (t) of 400, 500, 600, 700 and 800 ms; holding time (duration of clamping pressure exposure after USW, τ) of 3 s.

USW lap joints were fabricated using an 'UZPS-7' machine (SpetsmashSonic LLC, Russia). The overlap area of the joined PEI plates corresponded to the sonotrode sizes of 20×20 mm^2. The plates to be welded were placed in a fixing clamp, which excluded the possibility of their (mutual) movement during the USW process [24]. The layer shear strength (LSS) of the USW lap joints was assessed according to ASTM D5868. Since they were adherends that fractured in most of tensile tests, their cross section area of 20×2 mm^2 was taken in the calculations. In order to avoid (minimize) macroscopic bending of the lap joints during testing, gaskets in the form of PEI plates with a size of 20×2×60 mm were utilized.

The tests were carried out with an 'Instron 5582' electromechanical tensile testing machine. To examine the deformation behavior of the lap-joints, the Digital Image Correlation (DIC) method was utilized with the help of the "VIC 2D" software package (Correlated Solutions Inc., USA). For doing so, a speckle pattern was applied on the lateral surface of the samples, which was recorded under stretching using a digital camera "Point Grey Grasshopper 50S5M" (Point Grey Research ® Inc., Canada) with a CCD matrix "Sony ® ICX625" 2/3" 2448×2048 (resolution 5 megapixels, matrix size 8.4×7.0 mm, pixel size 3.45×3.45 microns). Strain values were computed at the rate of 5 Hz. The loading rate was 13 mm/min.

The structure the USW joints was analyzed over their cross-sections with a "Neophot 2" optical microscope (Carl Zeiss, Jena, Germany) equipped with a 'Canon 700D' digital single-lens reflex camera (Japan).

EXPERIMENTAL RESULTS

For quantitative comparison of the USW joints, their mechanical properties and dimensional characteristics were analyzed. In the first case, the tensile strength (σ_f) criterion was assessed (Fig. 1, a), while the second one was the USW joint thinning (Δd), measured by the contact method (with a screw caliper) at five points. It should be noted that the interlayer shear strength (LSS) was typically determined when assessing the quality of USW joints [25]. However, failure is to be guaranteed to occur adhesively along the fusion zone (between the adherends) in the studied cases. Since the neat PEI plates were welded, the USW joints could be fractured through the base material [26]. Respectively, the applied strength criterion was the σ_f parameter.

The formation of the USW joints is determined by the development of both frictional heating and penetration (mass transfer) processes at the interface of the components being welded [27]. However, the small (and somehow variable) thicknesses of the prepregs, combined with the high thermal conductivity of the CF-fabric, caused melting of the PEI binder in them and was accompanied by its partial extrusion under the action of clamping pressure during the USW procedures. Uniform flows of the molten PEI were impeded by the CF-fabric, causing the development of porosity (and local damage to the CF-fabric). Thus, it could not be expected that the macrostructure was uniform over the entire fusion zone area of 20×20 mm in the USW lap-joints (including on both sides of the prepregs, since the sonotrode energy was input only from one side upon US-welding). On this basis, average USW joint thinning values (measured in micrometers) were used as an integral dimensional parameter (Fig. 1, b).

According to Fig. 1, a, tensile strength of the USW joints with the prepreg characterized by the maximum CF-fabric content (at the PEI/CF-fabric ratio of 23/77) were greater than those for all other samples. Their maximum values reached 48.7 MPa at the USW duration of 500 ms. On the other hand, they were at the lowest levels of 12.7–28.6 MPa in the entire range of the applied USW durations at the minimum CF-fabric content (Fig. 1, a).

The dependences of the USW joint thinning on the USW durations were generally expected. At the PEI/CF-fabric ratio of 23/77, it changed slightly with increasing the USW durations due to the minimal possibility of extruding PEI, melted via frictional heating. At the same time, rising the USW durations was accompanied by a more than fourfold increase in the USW joint thinning (Fig. 1, b) at the maximum PEI content in the prepreg (for the same reasons).

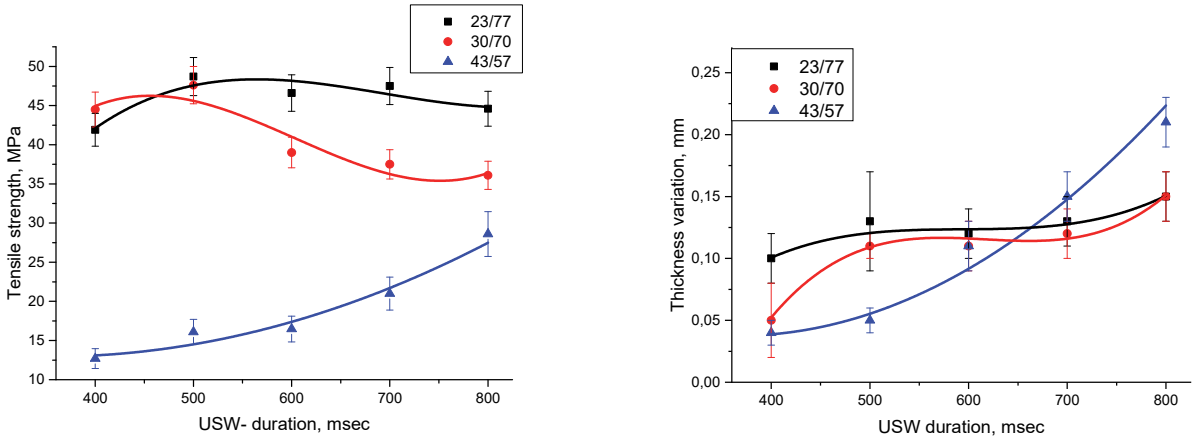

a b

Figure 1: The dependences of both tensile strength (a) and USW lap-joint thinning (b) values on the USW durations.

In order to understand the relationship between the mechanical properties and the (macro)structural characteristics, optical microscopy was implemented to investigate the cross-sections of the USW joints in the fusion zone. In addition to the qualitative comparison, 'CF-fabric layer' thicknesses (δ_{CFs}) were visually measured in Fig. 2 (this term was used by the authors to emphasize that the analyzed object was the cross-sectional area determined in the photographs and identified as the CF-fabric as a part of the prepregs). This parameter characterized the structural integrity maintenance when compared with the initial thicknesses of the prepregs and the CF-fabric in their compositions, since it could be compressed or widened ('swollen') and, accordingly, fractured due to extrusion of the molten PEI binder from the prepregs under the action of clamping pressure in the USW procedures. This fact was reflected by the curve of the USW joints with the thickest prepreg at the maximum binder content (the PEI/CF-fabric ratio of 43/57). At the minimum USW duration, the 'CF-fabric layer' thickness practically corresponded to that of the initial prepreg, whereas it was reduced due to 'mashing' of the prepreg at t = 600 and 700 ms. On the contrary, enhancing the 'CF-fabric layer' thickness was associated with the prepreg 'swelling' due to the intense interaction of the molten PEI binder with the damaged CF-fabric at t = 800 ms. These facts were confirmed in a number of optical images of the USW lap-joints, shown in Fig. 3.

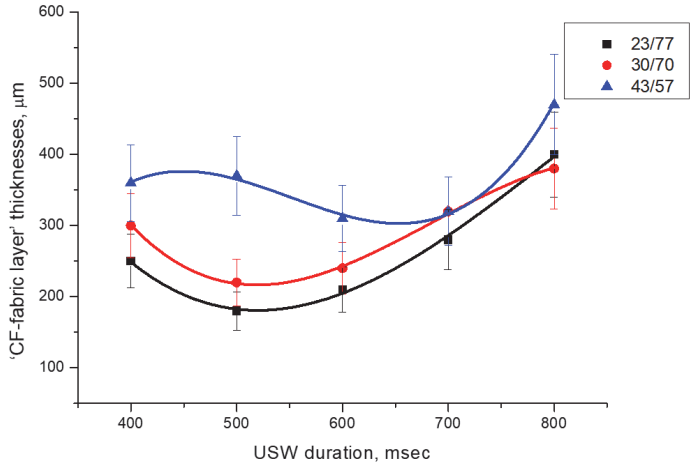

Figure 2: The dependences of the 'CF-fabric layer' thicknesses on the USW durations.

According to Fig. 3, the structure of the USW joints depended on the process durations: it was mostly uniform after short-term procedures lasting for 400–500 ms (Fig. 3, a–i), while longer USW time of 600–800 ms was accompanied by an effect similar to the CF-fabric 'swelling' in the prepregs. This result was generally consistent with the trend of the changes in tensile strength (Fig. 1, a), when this parameter predominantly depended on the PEI/CF-fabric ratios in the prepregs.

At t = 500 ms, the minimum 'CF-fabric layer' thickness was ~200 µm (Fig. 2). So, the prepreg slightly underwent deformation (mashing) during this short-term USW procedure. This fact corresponded to the formation of the USW lap-

joints, especially with the low PEI contents in the prepregs (Fig. 3, a and b). However, local discontinuities (such as interlayer cracks) were formed in the prepregs at the USW duration of 600 ms (especially with the high PEI contents), according to Fig. 3, h and i.

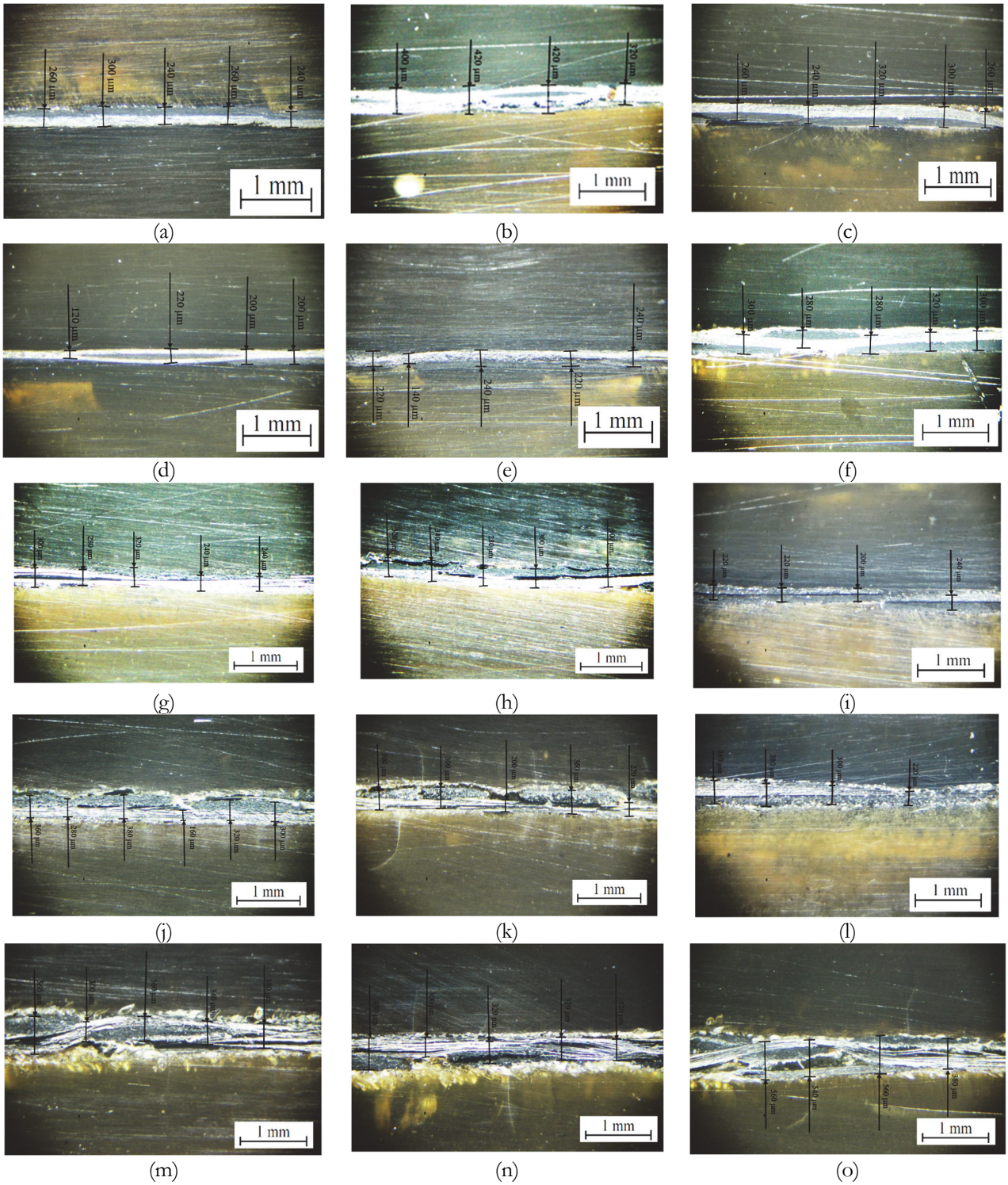

Figure 3: The optical images of the structure on the cross-sections of the USW joints for different combinations of the USW durations and the PEI/CF-fabric ratios in the prepregs; PEI/CF-fabric ratio of 23/77 (a,d,g,j,m); 30/70 (b,e,h,k,n); 43/57 (c,f,i,l,o); t = 400 ms (a,b,c); t = 500 ms (d,e,f); t = 600 ms (g,h,i); t = 800 ms (j,k,l); t = 800 ms (m,n,o).

Increasing the USW time up to 700 ms was accompanied by rising both the 'CF-fabric layer' thickness and the fusion zone width (Fig. 3, k–m). This phenomenon could be associated with greater frictional heating and the possibility of developing the mixing process in its bulk. The PEI adherends locally changed color in the area of contact with the prepregs, and cracked in some regions. It should be noted that the CF-fabric 'swelling' up to thicknesses of 280–320 μm progressed in the prepregs. In addition, local discontinuities were found at the interlayer boundary (Fig. 3, h and i). Nevertheless, it could be argued already at this stage of describing the obtained results that the number and sizes of the observed discontinuities did not correlate with the increased tensile strength levels (Fig. 1, a). This phenomenon is discussed below in more detail.

At the maximum USW duration of 800 ms (Fig. 3, k–m), the most heterogeneous and faulty structures of the USW lap-joints were formed, characterized by both the CF-fabric 'swelling' and cracking (fracturing) of the surface layer on the PEI adherends at the contact with the prepregs. The maximum 'CF-fabric layer' thickness exceeded 350 μm, surpassing all determined values for the applied USW durations.

Since the provided integral data on the structure (in fact, thickness) of the interface did not fully explain the reason for the difference in tensile strength of the USW lap-joints at various USW durations, a visual analysis of their general views (Fig. 4) was performed after the tensile tests. At the PEI/CF-fabric ratio of 43/57 and the USW durations of 400–700 ms, fracture occurred by the adhesion mechanism. This fact indicated that the required level of the interlayer strength was not achieved (Fig. 4, c, e, i and l). Only for the USW duration of 800 ms, fracture surfaces were characterized by a mixed adhesive-cohesive character (Fig. 4, o) at $\sigma > 27$ MPa. According to the authors, this phenomenon was caused by the formation of the wide fusion zone, partially reinforced with the locally damaged CF-fabric.

With lowering the PEI content in the prepregs, the mixed adhesive-cohesive fracture pattern predominated. In this case, the main crack initiated at one of the joined PEI adherends and propagated over a certain distance, contributing to macrobending of the sample (such a phenomenon is clearly demonstrated below in Section 4 devoted to computer simulation). This deformation behavior resulted in cohesive fracture of the USW lap-joints (Fig. 4, a, b, d, e, g, h, j, l, n and o).

Since the key objective of the study was to determine the relationship between the (macro)structure of the USW lap-joints and their mechanical properties, the results of testing samples with the minimum PEI/CF-fabric ratio of 23/77 are discussed below in more detail. According to Fig. 3, a, d, g, j and n, rising the USW durations from 400 up to 800 ms radically changed the structure of the fusion zone. However, tensile strength did not vary significantly, being in the range of 42–48 MPa. Respectively, the optimization of the USW parameters should not be based on enhancing tensile strength only, the magnitude of which was determined by a number of factors, including adhesive strength (whose value, unfortunately, could not be assessed). According to the authors, the increase in adhesive strength at the great USW durations of 700–800 ms was associated with additional reinforcement of the fusion zone with the partially fractured CF-fabric.

When application time of ultrasonic vibrations exceeded a certain threshold, melting and spreading of the polymer binder occurred in the prepreg. In doing so, the carbon fibers in the prepreg were flown together with the molten polymer. The mixing of the fibers, relative to their initial location could give rise to increasing the contact area and the LSS as well.

Obviously, it was necessary to ensure minimal damage to both the PEI adherends and the prepreg in the fusion zone [28, 29]. This was especially true under cyclic loads, leading to premature failure of the USW lap-joints [24].

In order to analyze the effect of the PEI/CF-fabric ratio in the prepregs on the deformation response of the USW lap-joints, considering the interlayer adhesion level, FEM-based computer simulations were carried out. Their goal was to show the fact of the development of macroscopic bending [30], as well as to identify the processes preceding the onset of the fracture processes.

As shown above, the structure of the USW lap-joints was not uniform, depending on i) variations in the prepreg thicknesses; ii) differences in thermal conductivity of the CF-fabric and PEI; iii) different pattern of melting and extrusion of the polymer in the center and at the periphery of the fusion zone, etc. Several structural factors influencing the development of deformation of the USW lap-joints were highlighted above. For a qualitative analysis of the structure of the fusion zone in the USW lap-joint obtained using the most rational parameters (the PEI/CF-fabric ratio of 23/77 and the USW duration of 500 ms), its computed tomography (CT) was carried out, the results of which are shown in Fig. 5 in the form of planar sections. As expected, the structure of the PEI plates did not change in the fusion zone (Fig. 5, a and f). At the PEI plate/prepreg interface (mainly in the upper part), a number of micropores were found (Fig. 5, b, d and e), while the CF-fabric retained its structural integrity in the prepreg (Fig. 5, c and d).

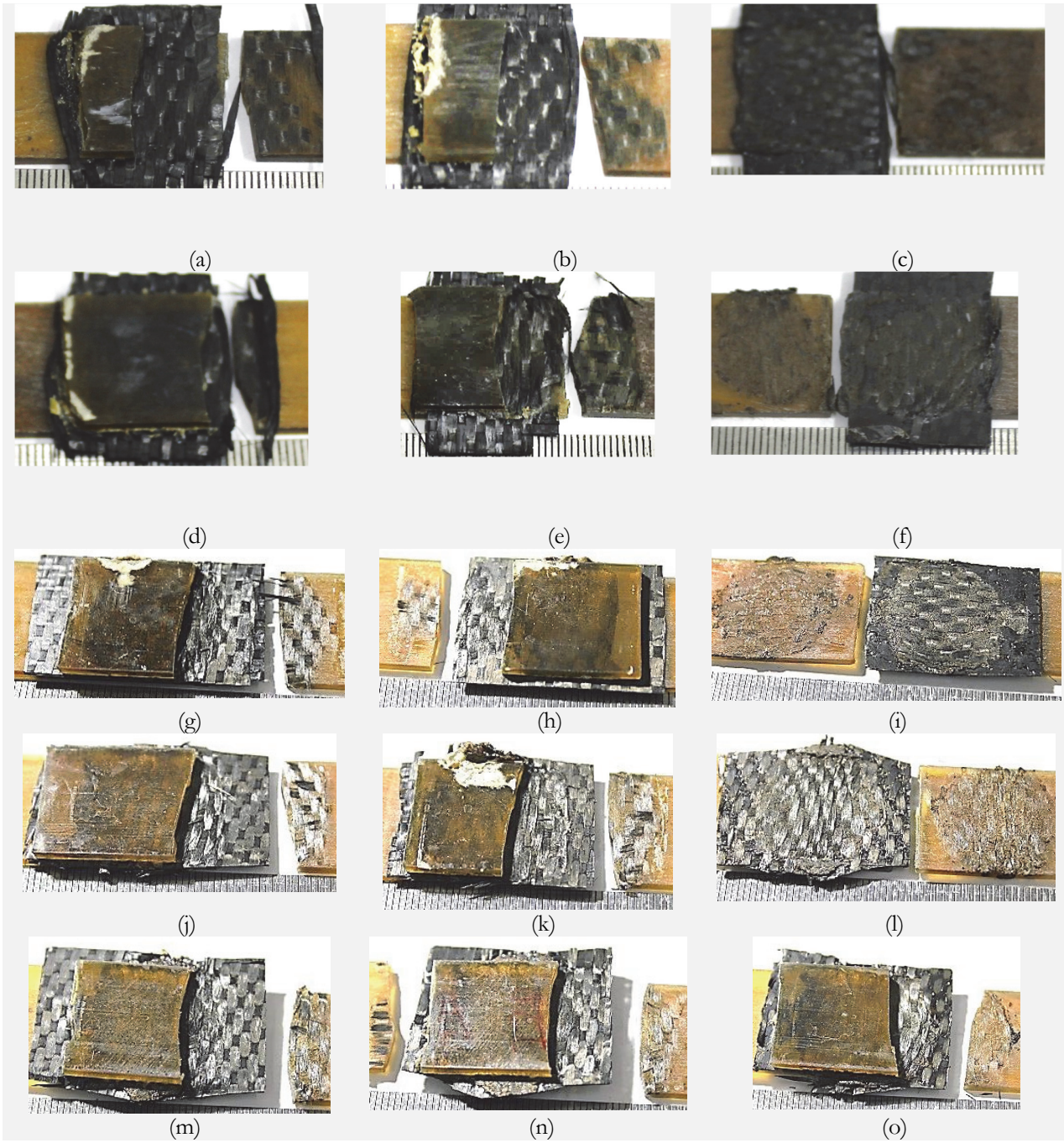

Figure 4: The general views of the USW joints after the shear tests; PEI/CF-fabric ratio of 23/77 (a,d,g,j,m); 30/70 (b,e,h,k,n); 43/57 (c,f,i,l,o); t = 400 ms (a,b,c); t = 500 ms (d,e,f); t = 600 ms (g,h,i); t = 800 ms (j,k,l); t = 800 ms (m,n,o)

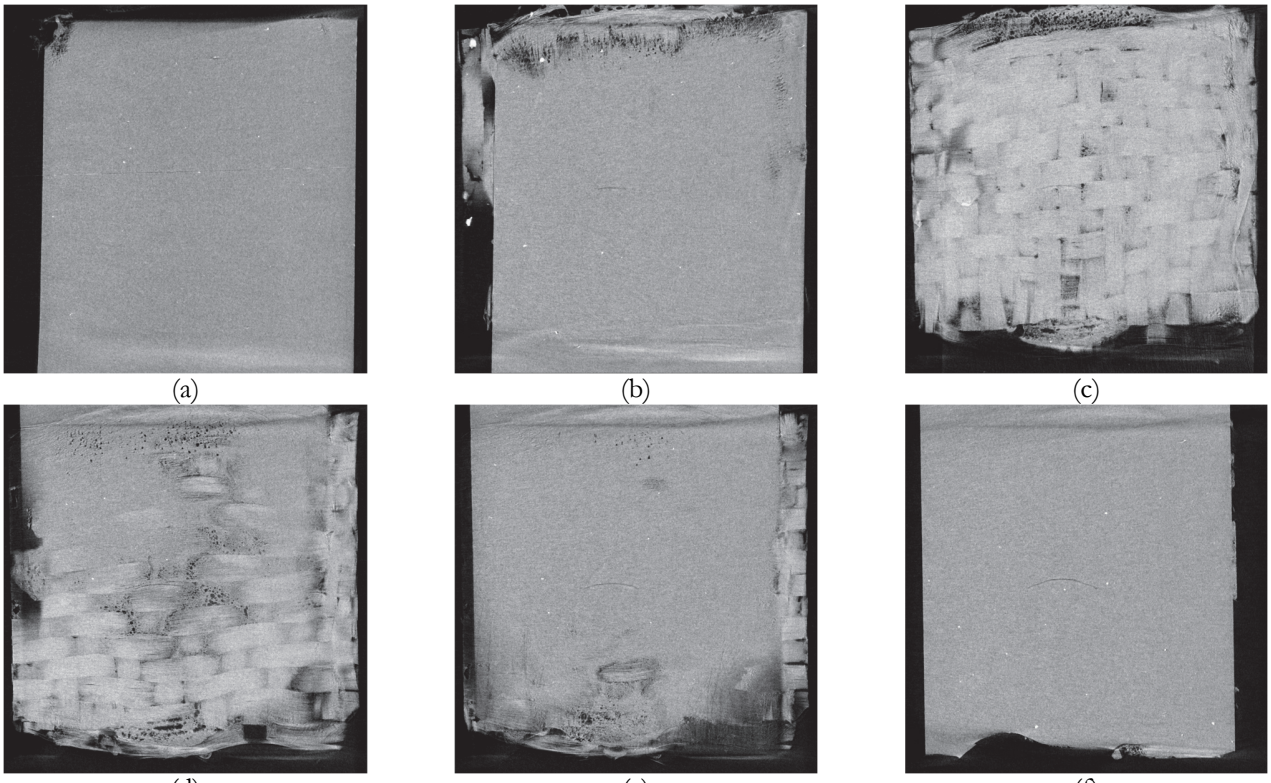

Figure 5: The CT micrographs obtained for the USW lap-joint formed at the PEI/CF-fabric ratio of 23/77 and the USW duration of 500 ms

COMPUTATIONAL EXPERIMENTS OF THE USW LAP-JOINTS WITH DIFFERENT ADHESION LEVELS

Statement of the computer simulation problem

A theoretical study of the effect of the interfacial adhesion level on the tensile strength of the USW lap-joints was carried out using the 'ABAQUS 2019' FEM-based software package (Dassault Systemes, France). Fig. 6 shows a scheme of the computational domain for 3D modeling of the USW lap-joints of two PEI adherends with dimensions of 45×20×2.2 mm and the contact area of 20×20 mm, similar to the experimental data described above. The model reproduced only part of the samples without the areas located in the clamps of the testing machine. Between the PEI adherends, there was a prepreg layer consisting of the CF-fabric impregnated with PEI.

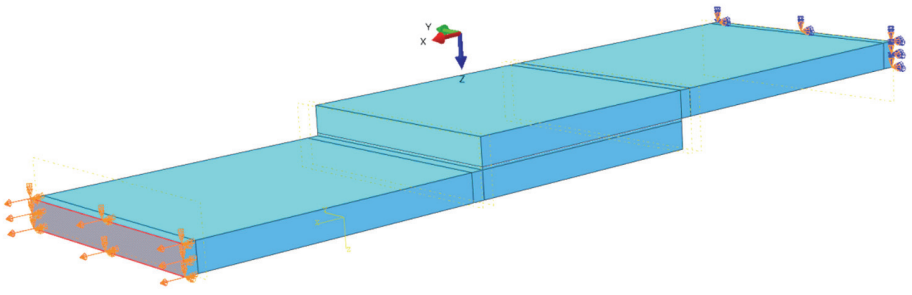

Figure 6: The scheme of the computational domain for 3D modeling of the USW lap-joints.

The following boundary conditions were accepted for the model:
- the left end of the sample was rigidly fixed, so displacements in all directions were prohibited;
- on the right end, movements in the direction of the Ox axis were specified step by step; displacements at the end along other axes were prohibited;

- all other ends were free.

The PEI properties were taken according to experimental data by the authors [24]. In doing so, the loading diagram possessed nonlinear pattern that was taken into account in the calculations. The following mechanical properties were taken: modulus of elasticity of 2055 MPa, Poisson′s ratio of 0.3, the tensile strength of 123 MPa, elongation at break of 9.9%.

The prepreg was modeled over its equivalent properties, i.e. without explicitly considering the reinforcing CF-fabric. Its physical properties (such as elastic and shear moduli, as well as the tensile strength) were calculated analytically using the formulas for plastics unidirectionally reinforced with CFs [31, 32]. Its behavior was taken as elastic.

The transverse modulus of elasticity and strength were determined as:

$$E_{33} = \frac{E_{\text{PEI}} E_{\text{CF}}}{\varphi E_{\text{PEI}} + (1-\varphi) E_{\text{CF}}};\ \sigma_{33} = \frac{\sigma_{PEI}}{(1-\varphi)} \tag{1}$$

Longitudinal (in the reinforcement plane) modulus of elasticity was assessed as:

$$E_{11} = E_{22} = E_{\text{CF}} \cdot \varphi^* + E_{33} \cdot (1-\varphi^*) \tag{2}$$

The tensile strength in the reinforcement direction was calculated as:

$$\sigma_L = \sigma_{CF} \cdot \varphi^* + \sigma_{PEI} \cdot (1-\varphi^*) \tag{3}$$

where E_{CF} and E_{PEI} were moduli of elasticity of the CF-fabric and PEI, respectively; σ_{CF} and σ_{PEI} were their shear strength values in the corresponding direction; φ^* was the PEI/CF-fabric ratio.

The shear modulus was calculated using the following formula:

$$G_{13} = G_{23} = \frac{G_{м} G_{в}}{\varphi G_{м} + (1-\varphi) G_{в}} \tag{4}$$

$$G_{12} = G_{\text{B}} \cdot \varphi^* + G_{\text{м}} \cdot (1-\varphi^*) \tag{5}$$

Poisson′s ratios:

$$\mu_1 = \mu_2 = \mu_{\text{в}} \cdot \varphi + \mu_{\text{м}} \cdot (1-\varphi) \tag{6}$$

$$\mu_3 = \frac{\mu_1 E_1}{E_3} \tag{7}$$

The tensile strength of CFs was 4.9 GPa, while their modulus of elasticity was 240 GPa. As in the experiment, the prepreg thicknesses varied from 250 up to 350 μm depending on the PEI/CF-fabric ratios. The corresponding prepreg properties are given in Tab. 1 for various PEI/CF-fabric ratios.

To determine the parameters of the stress-strain state, the contact problem of elasticity theory was solved in a three-dimensional static statement, taking into account geometric and physical nonlinearity. The finite element method (FEM) was utilized with the help of the Abaqus/Standart CAE 2019 software package. When constructing the FEM model, C3D8R volumetric tetrahedral elements with linear approximation of displacements were used. The number of nodes in the model was 520228, the number of elements was 213404, the number of elements at the contact boundaries was 40804.

At the plates and prepreg interface, tangential contact was set without taking friction into account. In doing so, a "Hard contact" condition was chosen for normal contact. The latter prohibited mutual penetration of contacting bodies. The "coupling – separation" condition on the contact sites was set using "Cohesive behavior" option, which allowed one to set the “Damage” conditions on the contact. The latter represented the separating criterion (*d*) in the form of: i) a stress level

(adhesion) or displacement, or ii) ideal adhesion. To implement further separation, the evolution criterion in the form of "Displacement at failure" was used.
The fracture in the plates and prepregs was defined in the form of the nucleation and propagation of cracks. The latter was implemented using the extended finite element method (XFEM). The criteria for the cracks origin was the achievement of maximum stresses, as which the ultimate strength of the corresponding materials were selected. To implement further cracking, an evolution criterion in the form of "Total/Plastic displacement" was used.

Prepreg properties	PEI/CF-fabric ratio (prepreg thickness)		
	25/75 (250 μm)	35/65 (300 μm)	45/55 (350 μm)
Longitudinal tensile moduli of elasticity, E_{11} and E_{22} (GPa)	95	80	70
Transverse tensile modulus, E_{33} (GPa)	8	5.8	4.5
Shear moduli, G_{13} and G_{23} (GPa)	3.1	2.2	1.8
Shear modulus, G_{12} (GPa)	38	36	28.8
Poisson's ratios, μ_1 and μ_2	0.225	0.24	0.26
Poisson's ratio, μ_3	0.019	0.017	0.0167
Tensile strength in the reinforcement direction, σ_{11} and σ_{22} (GPa)	2.15	1.70	1.50
Tensile strength across the reinforcement direction, σ_{33} (GPa)	0.492	0.358	0.270

Table 1: The mechanical properties of the prepregs with various PEI/CF-fabric ratios.

The tensile strength values of the USW lap-joints were calculated for the specified range of the prepreg thicknesses (h) at interlayer adhesion levels from 5 up to 60 MPa. For comparison, ideal adhesion was also considered. The criterion for failure of the sample as a whole was the development (onset) of shear between two contacting bodies or initiation of a crack in them. For the given both model and material properties, the following results were obtained.

The results of computer simulation and their discussion

The numerical investigations showed that strain–stress curves coincided at the same adhesion levels but different both prepreg thicknesses and the corresponding PEI/CF-fabric ratios in the prepregs (Tab. 1). This phenomenon was caused by the fact that the moduli of elasticity of the prepregs, primarily the shear modulus, differed by an order of magnitude from those of the PEI adherends despite the changes in the PEI/CF-fabric ratios. A significant decrease in the moduli could reflect bending of individual CFs during the USW [33].
In this regard, calculations were carried out for ideal adhesion with varying the modulus of elasticity of the prepreg along the reinforcement direction from 20 up to 80 GPa, as well as for conditions of isotropic elastic properties of the prepreg equal to those for PEI (2 GPa). The obtained results are shown in Fig. 7.
According to the above dependencies, a 2-fold change in the elastic modulus of the prepreg practically did not affect the slope of the loading diagram (tensile stiffness of the sample), since when the lap joint was stretched, the load was applied directly to the plates. Thus, the prepreg mostly played a binding function, increasing the stiffness and strength of the joint area. Therefore, the change in its stiffness insignificantly affected the tensile stiffness of the sample. When the elastic modulus of the prepreg decreased to the level of the plate's modulus ~2 GPa, which was 40 times less than the calculated value for the prepreg ~ 80 GPa (Tab. 1), the slope of the loading diagram, characterizing the stiffness of the sample as a whole, decreased slightly (by 12.5%). In doing so, the stiffness of the sample became equal to the stiffness of the plates. This indirectly confirmed the correctness of the employed FE model. Since we aimed at evaluating only the effect of changes in the elastic modulus of the prepreg on sample stiffness variation, the strength was not varied, being correspondent to one of the prepreg with a thickness of 300 μm (1.7 GPa). This does not correspond to the real material. Therefore, the strength assessment was not carried out in this case, but the fracture pattern was considered for the different stiffness of the prepreg. Pictograms of the stress distribution are shown next to the curves, which showed fracture pattern in the joint area. The threefold displacement scaling was applied.

In the case of the prepreg with the anisotropic properties (in the range of 20–80 GPa), fracture of the PEI adherends began at the corners of the USW lap-joints due to their deformation in the transverse direction outside the fusion zone. So, the stiffer prepreg was not deformed, causing large strains in these regions. With the isotropic properties of the prepreg (2 GPa), a crack propagated in the PEI adherends along the edge of the USW lap-joints due to their stretching and bending. The effect of prepreg stiffness on the slope of the loading diagrams under tension showed that it might be one of the reasons for the slope variation of the experimental curves. Despite the insignificant effect of prepreg stiffness on the slope of the loading diagrams, its decrease could substantially affect the strength during bending tests. Therefore, reducing the stiffness does not make sense.

In the tensile tests of the USW lap-joints, the prepreg thickness did not affect the mechanical properties (if other characteristics of the prepreg and its adhesion level to the PEI adherends were constant). In this regard, the prepreg thickness of 300 μm was considered for deeper investigations of the effect of the adhesion levels on the tensile strength of the USW lap-joints.

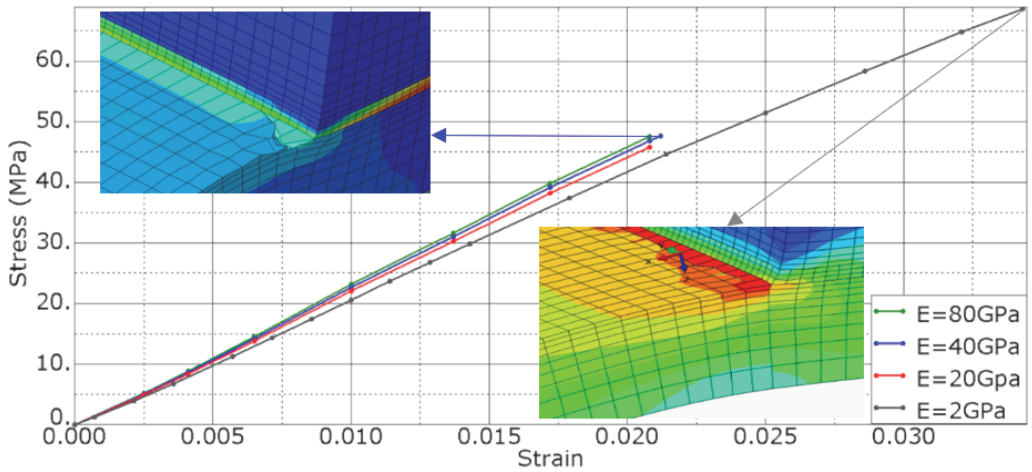

Figure 7: The strain–stress diagrams for the USW lap-joints with the prepreg thickness of 300 μm and ideal adhesion, the modulus of elasticity of the prepregs along the reinforcement direction is varied from 20 up to 80 GPa; the threefold displacement scaling was applied.

Fig. 8 shows strain–stress diagrams for the USW lap-joints with the prepreg thickness of 300 μm at the adhesion levels from 5 up to 60 MPa. It is seen that the strength varied slightly with increasing the adhesion level above 30 MPa, while the dependence practically coincided with that at ideal adhesion at 60 MPa. For doing so, the level of 60 MPa was taken as the calculations limit. Pictograms of the strain distribution are shown next to the curves, which illustrated the fracture pattern in the lap joint area. It is seen that the greatest strains took place in the plates in all the cases, while the fracture pattern varied significantly. Three-fold scaling of the offset was applied.

As the adhesion level decreased, the tensile strength of the USW joint reduced as well, changing the fracture mechanisms, shown in Figs. 9 and 10. Values of both normal and shear stresses in the fusion zone were taken as the adhesion levels. Since the USW lap-joints fractured due to the development of shear stresses, their levels were applied firstly. The range of strength values obtained at different adhesion level correlated with the experimental values shown in Fig. 1,a. The obtained results showed that the prepreg-to-plates adhesion was the key strength determining parameter. In the experiments, its value was determined by the welding time and the thickness of the prepreg.

As an instance, Fig. 9 presents the distribution patterns of the maximum principal stresses and strains at 5 MPa. An analysis of the stress distribution in the USW lap-joints (Fig. 9) enabled to conclude that the maximum stresses were concentrated in the prepreg, while the maximum strains were in the PEI adherend, symmetrically on both sides of the delamination area (indicated by a red square in Fig. 9, b). According to Fig. 9, c, the PEI adherends were bent even at low adhesion levels. In the bending region, plastic strains developed in the PEI adherends, contributing to initiation of cracks. In order to illustrate the presence and pattern of the bend in Fig. 9, b and c (as well as in all figures presented below), the threefold displacement scaling was applied, which also made it possible to visualize the development of plastic strains.

At an adhesion level of 15 MPa, the delamination process developed firstly (highlighted by a red frame in Fig. 10, a and on the right side along the edge of the USW lap-joint). Then, cracks initiated symmetrically in both PEI plates (shown in the bottom one for example) and gradually propagated towards the center of the fusion zone. With ideal adhesion (that reflected

the impossibility of delamination), the fracture process was caused by initiation and propagation of cracks in the PEI adherends.

Fig. 10, b and c shows distributions of the maximum strains at ideal adhesion, while Fig. 10, a and b visualizes bending of the PEI adherends due to the Poisson effect. In this case, both the prepreg and the top PEI plate were practically not compressed. This fact gave rise to large strains of the bottom PEI adherend at the corners of the USW lap-joint, where the fracture process began. At an adhesion level of 30 MPa and above, failure occurred due to initiation and propagation of cracks in the PEI plates, as with ideal adhesion. In the latter cases, plastic strains were higher than those at the minimum adhesion level of 5 MPa.

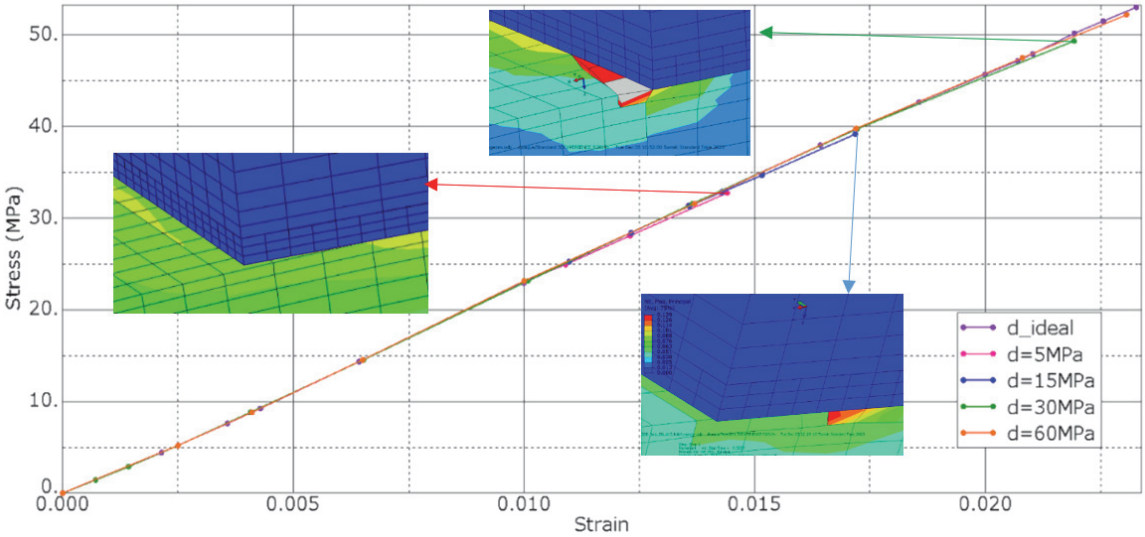

Figure 8: The strain–stress diagrams for the USW lap-joints at the adhesion levels from 5 up to 60 MPa.

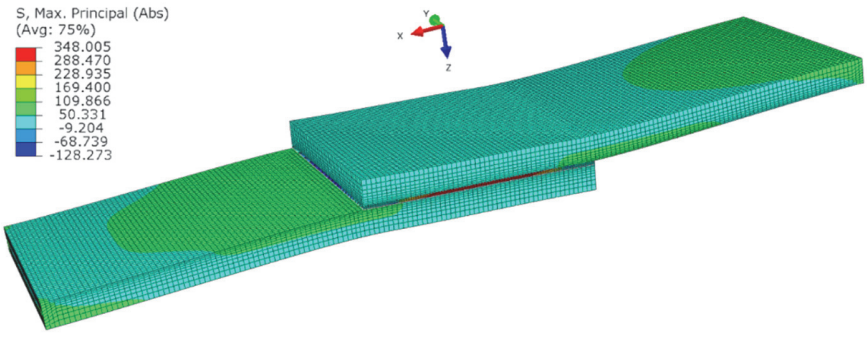

a)

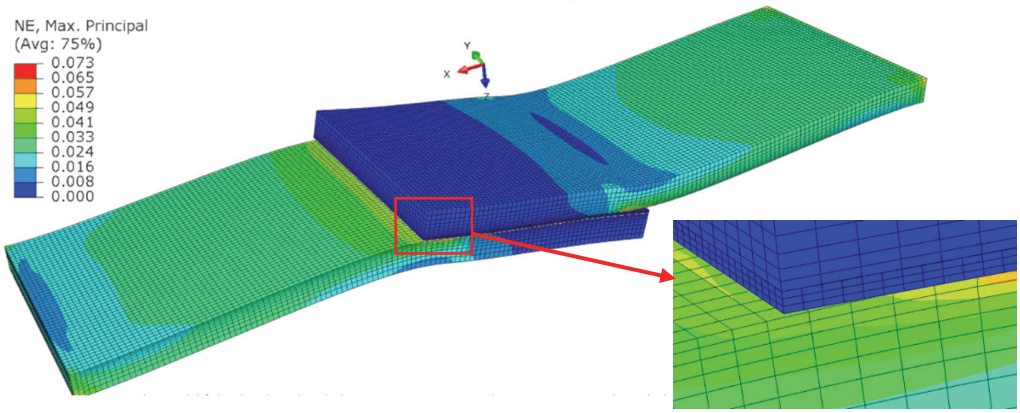

b)

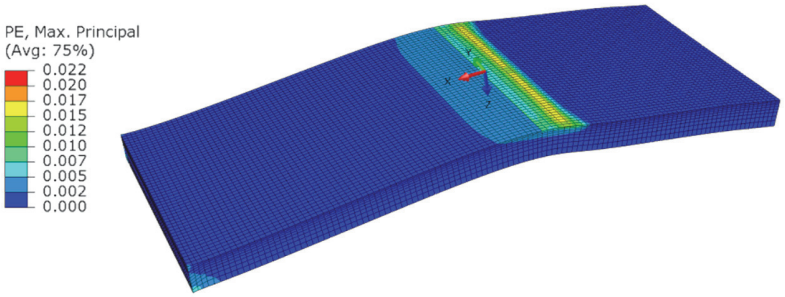

c)

Figure 9: The distributions of the maximum principal stresses (a) and strains (b) in the USW joints, as well as plastic strains in the PEI adherend (c) at the adhesion level of 5 MPa (corresponding to the onset of fracture).

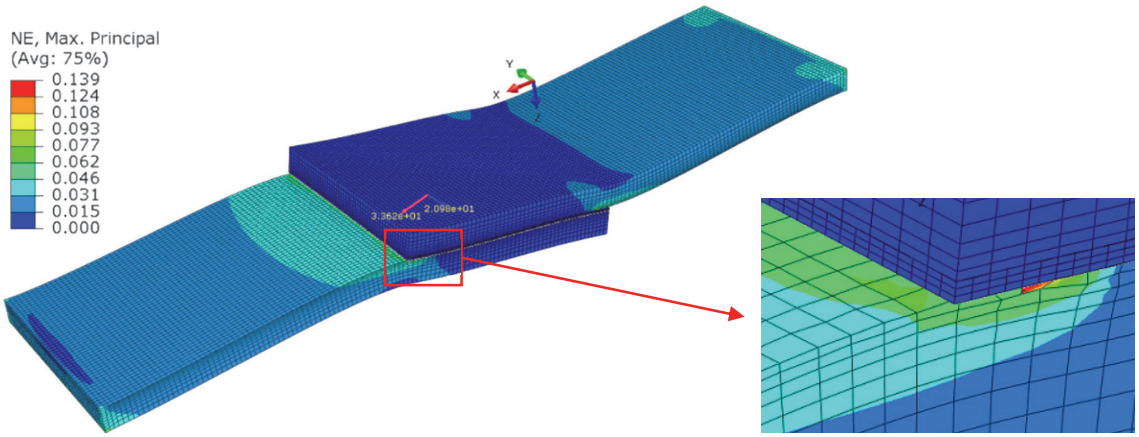

a)

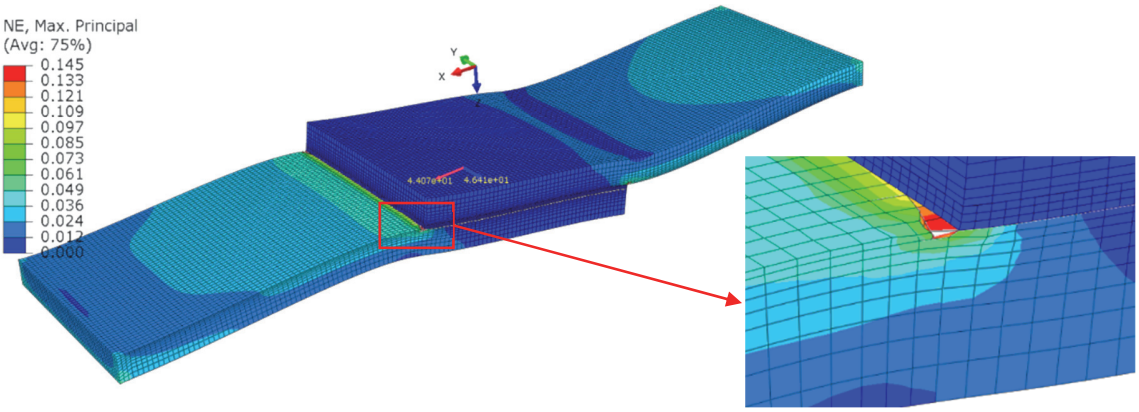

b)

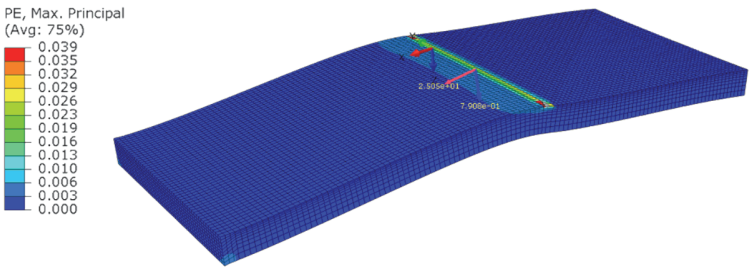

c)

Figure 10: The distributions of the maximum principal strains in the USW lap-joint at the moment of failure at the adhesion level of 15 MPa (a) and at ideal adhesion (b), and plastic strains in the PEI adherend (c); the threefold displacement scaling was applied.

Thereby, different adhesion levels in combination with the preset PEI properties and the dimensions of the USW lap-joints determined the tensile strength (Fig. 9) and the fracture mechanism:

- At the low adhesion levels (Fig. 9, b and d), delamination occurred in the areas of the PEI plates with the maximum stresses (namely at the edges/corners of the USW lap-joints). As a result, such stresses were reduced without giving rise to large plastic strains (Fig. 9, b). With further loading, the USW lap-joints fractured by the delamination mechanism (Fig. 9, b).
- At the average adhesion levels, bending of the PEI adherends increased upon loading. Then, delamination was typically observed. In these areas, stresses were reduced without the development of great plastic strains. With further loading, macroscopic bending intensified and, despite gradual delamination, resulted in the accumulation of plastic strains (Fig. 10, b and d). This process was accompanied by initiation of cracks in the PEI plates on both sides of the USW lap-joints (Fig. 10, a), causing their failure.
- At the high adhesion levels, bending of the PEI adherends enhanced with loading that resulted in their cracking precisely in the curved area on both sides of the USW lap-joints due to the development of large plastic strains (Fig. 10, b–d).

Along with these reasons, the tensile strength of the USW lap-joints was also significantly affected by the development of transverse strains of the PEI plates outside the fusion zone (Figs. 9, b; 10, b and c). This phenomenon led to their narrowing due to the Poisson effect in the bending area in front of the USW lap-joints. As a result, great strain gradients were occurred at the corners of the USW lap-joints between the incompressible prepreg and the PEI adherends, which were compressed in the transverse direction because of different stiffnesses. Typically, fracture began in such areas.

OPTIMIZATION OF THE USW PARAMETERS

As a discussion, the authors considered it necessary to focus on the analysis of the factors that affected the mechanical properties and the dimensional characteristics of the USW lap-joints in the context of their multi-criteria optimization. From the standpoint of ensuring their strength according to the criterion of the maximum tensile strength, the prepreg with the minimum PEI content turned out to be the most effective. In the range of the USW durations from 400 up to 800 ms, these values were comparable, although the maximum tensile strength were registered at t = 500 ms. In this case, the CF-fabric was intact after the USW procedure, which was consistent with the USW lap-joint thinning of 100–130 μm (Fig. 1, b).

Therefore, the USW parameters had to be optimized considering a number of the mechanical properties and the dimensional characteristics, among which the following had to be highlighted:

1. High levels of tensile strength (above 45 MPa) had to be achieved.
2. USW durations had to be within 600 ms, so that extruded flows of the molten binder did not damage the CF-fabric, and also ensured the surfaces' integrity of the PEI plates adjacent to the prepreg. However, this boundary condition was a restriction on the input (control) parameter, while the authors needed to determine the ranges of values of the functional characteristics of the USW lap-joints, i.e. namely the output ones.
3. The USW lap-joint thinning had to be at least 100 μm for the formation of USW joints, but below 130 μm to avoid (minimize) damage to the prepreg.
4. Changes in the 'CF-fabric layer' thickness relative to its initial value in the original prepreg had to be negative (to prevent the prepreg 'swelling'), while its thinning by more than 100 μm was also unacceptable, according to the considerations for the prepreg integrity maintenance (Figs. 2 and 3).

To optimize the prepreg thicknesses and the USW parameters, the Response Surface Methodology (RSM) approach was applied [34, 35]. For this purpose, surfaces of the mechanical properties and the dimensional characteristics (parameters) were drawn (Figs. 11–13; values along the axes were normalized), based on interpolation of the experimental data presented in Tabs. 2–4.

Based on the obtained surfaces, a summarizing region was drawn (shaded in green in Fig. 14), enabling to determine the range of the optimal parameters (the USW durations and the PEI/CF-fabric ratios) necessary to obtain USW lap-joints, characterized by high strength and low-defect structure (with minimal damage to the prepreg). The summarizing region showed that those with the PEI/CF-fabric ratios less than 30/70 and the USW durations of 400–600 ms were acceptable. It should be noted that a lower PEI content in the prepreg was not practically possible, since the minimum binder contents were at least 30 wt. % in typical industrially produced ones.

USW duration, ms	PEI/CF-fabric ratio		
	23/77	30/70	43/57
400	41.9	44.5	12.7
500	48.7	47.6	16.1
600	46.6	39.0	16.5
700	47.5	37.5	21.0
800	44.6	36.1	28.6

Table 2: Tensile strength levels for different USW duration vs PEI/CF-fabric ration combinations.

USW duration, ms	PEI/CF-fabric ratio		
	23/77	30/70	43/57
400	0.10	0.05	0.04
500	0.13	0.11	0.05
600	0.12	0.11	0.11
700	0.13	0.12	0.15
800	0.15	0.15	0.21

Table 3: The USW lap-joint thinning values for different USW duration vs PEI/CF-fabric ration combinations.

USW duration, ms	PEI/CF-fabric ratio		
	23/77	30/70	43/57
400	0	+0	-50
500	-50	-40	-100
600	+50	-20	-150
700	+80	+40	+20
800	+140	+80	+120

Table 4: Mean changes in the 'CF-fabric layer' thickness for different USW duration vs PEI/CF-fabric ratio combinations.

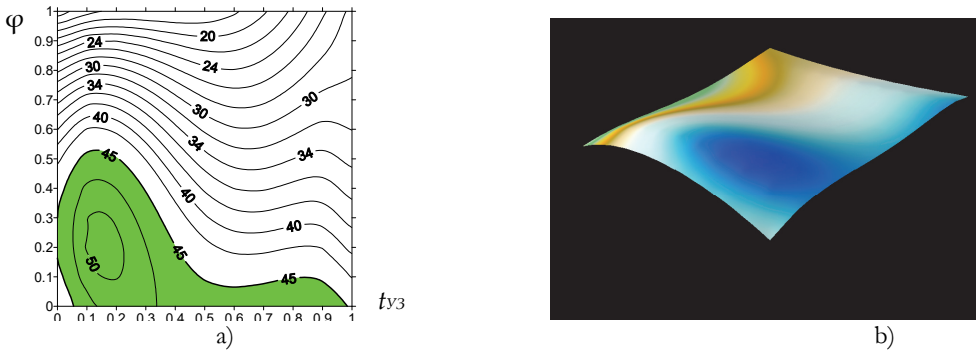

Figure 11: The tensile strength vs USW duration dependences.

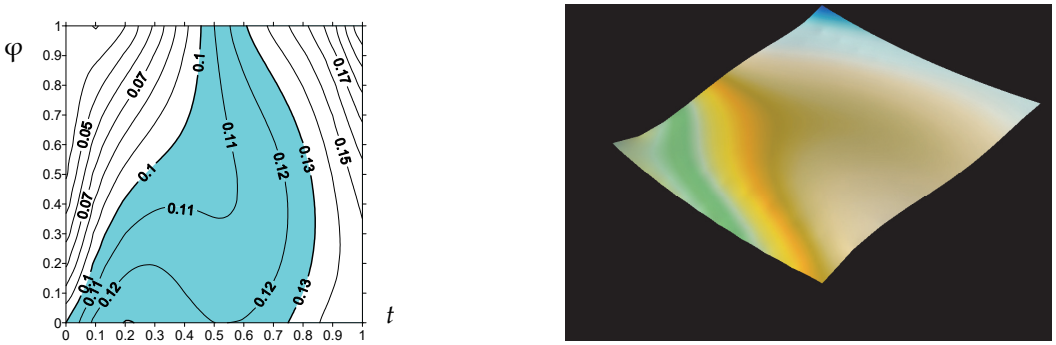

a) b)

Figure 12: The USW joint thinning vs USW duration dependences.

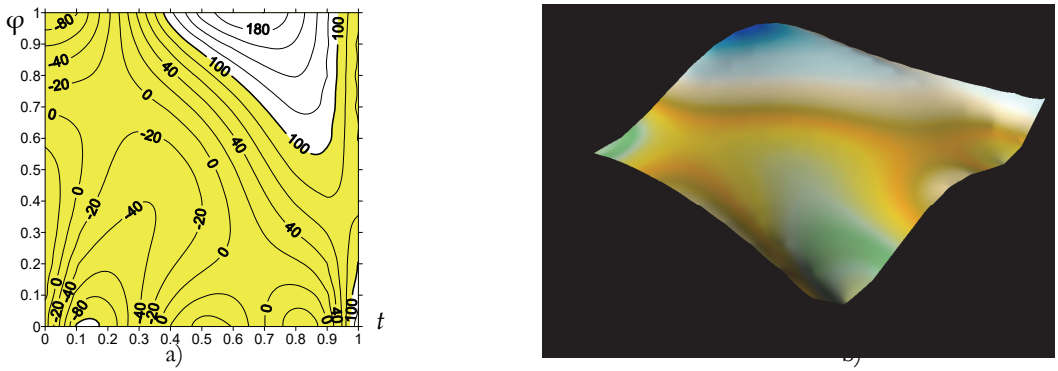

a)

Figure 13: The 'CF-fabric layer' thickness vs USW duration dependences.

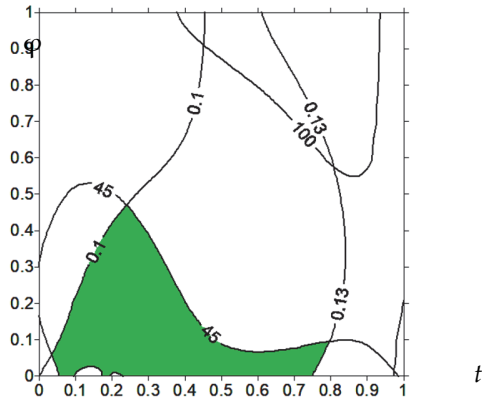

Figure 14: The integral prepreg characteristics vs the USW durations and the prepreg thicknesses.

MANUFACTURE OF LAMINATES BY USW

For continuing the discussion of the obtained results and confirming the possibility of fabricating laminates by the USW procedures, the authors compared the mechanical properties of ones made by compression molding (CM) and the USW technique. The evaluation was based on the results of the conventional short beam interlaminar shear test for laminates (ISO 14130:1997). In the fabrication of a sample by the CM method, the prepreg with the PEI/CF-fabric ratio of 43/57 wt.% was used. Upon the CM process, seven layers of the prepreg laid in a stack were compressed at a pressure of 0.5 MPa and a temperature of 320 °C.

In the USW procedure, the parameters determined in the previous section were implemented: the USW duration of 520 ms, the PEI/CF-fabric ration of 23/77 (which approximately corresponded to the middle of the green area in Fig. 14). As in

the previous experiments, clamping pressure was 1.7 atm and holding time was 3 s. For comparison, another sample was fabricated using the prepreg with the PEI/CF-fabric ratio of 57/43 at t = 750 ms. From the samples of the seven-layer laminates, beams with dimensions of 20×10×2 mm were cut made with a vertical CNC milling machine.

Fig. 15 shows a diagram characterizing the LSS values of the studied laminates. For the CM ones, the maximum achieved levels were ~60 MPa, while relatively low values were observed for the samples fabricated by the USW procedures. However, increasing the USW duration up to 750 ms enhanced the LSS values above 40 MPa.

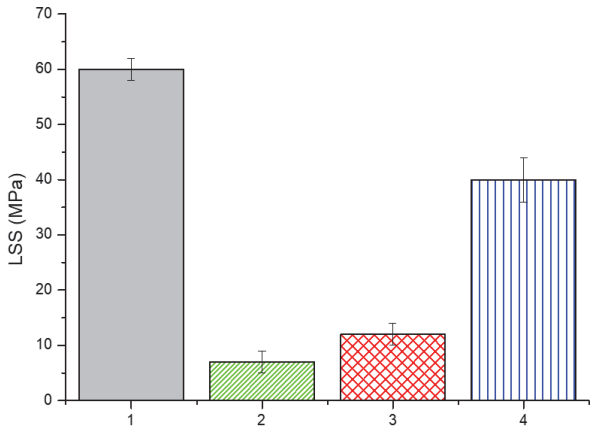

Figure 15: The LSS values for the laminates fabricated by: 1 – CM; 2 – USW, t = 520 ms, PEI/CF-fabric ratio of 23/77; 3 – USW, t = 520 ms, PEI/CF-fabric ratio of 43/57; 4 – USW, t = 7520 ms, PEI/CF-fabric ratio of 43/57.

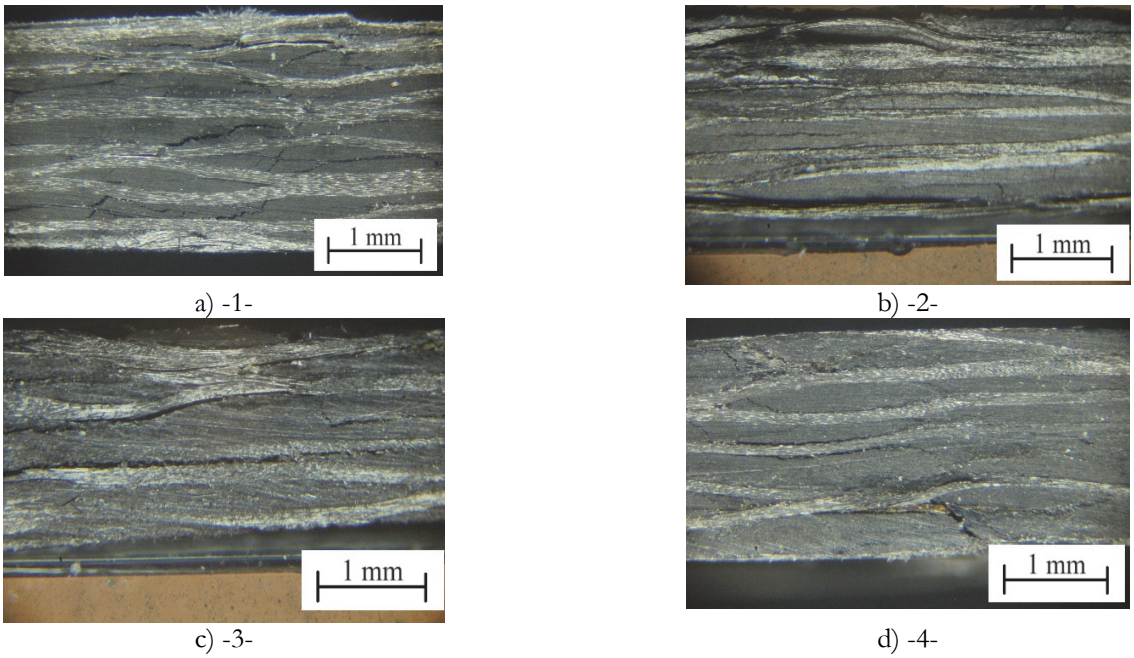

a) -1- b) -2-

c) -3- d) -4-

Figure 16: The cross-sections of the laminates after the three-point bending tests; CM (a); USW (b–d): 2 – t=520 ms, PEI/CF-fabric ratio of 77/23 (b); 3 – t=520 ms, PEI/CF-fabric ratio of 57/43 (c); 4 – t=750 ms, PEI/CF-fabric ratio of 57/43 (d).

An analysis of the structure of the laminates showed that the prepregs manufactured under the laboratory conditions were not always characterized by the thickness uniformity and the identical degree of impregnation along the entire length of the samples. This heterogeneity was 'inherited' during the manufacture of the seven-layer laminates (Fig. 16). In addition, some variations in the binder contents were observed in different sections of the prepregs. Laying in the stack of rectangular fragments in the mold could cause uneven polymer spreading even under the low-pressure conditions (0.5 MPa) during the CM process. This phenomenon resulted in some heterogeneity of the macrostructure as well. According to Fig. 16, a, interlaminar cracks were formed in binder-enriched regions during the three-point bending tests. However, the achieved

LSS levels for the laminates containing the laboratory-made prepregs were quite high. It should be noted that the specificity of manufacturing the laminates by the USW procedures was not only the layer-by-layer joining of the prepregs [36].

The sonotrode sizes of 20×20 mm did not allow the consolidation process to be carried out simultaneously along the entire length of the 60 mm long prepregs. Therefore, the USW procedures were carried out in three sequentially located sections in the 'spot welding' mode. Unfortunately, this process could be accompanied by the formation of a heterogeneous structure at the junction of these sections.

An analysis of the cross-sectional images of the USW laminates showed that the USW duration of 520 ms was insufficient to to consolidate prepregs regardless of the component ratios in them (Fig. 16, b and c). Respectively, the LSS level was insufficient (Fig. 14). At the USW duration of 750 ms, it was possible to ensure reliable joining of such prepregs (Fig. 16, d) and the high LSS level was observed at the PEI/CF-fabric ratio of 57/43. It should be noted that the USW parameters optimized in Section 5 differed from those, enabling to form the prepreg-joint in this case. According to the authors, the reason was a significant difference in the nature of the transmission of ultrasonic vibrations through the PEI plate (adherend) with 2 mm thick, in contrast to the thin (but significantly more durable) prepreg, the basis of which was the reinforcing CF-fabric.

The authors had to note that advanced USW procedures for manufacturing laminates from prepregs should be developed as a continuous process in subsequent studies. However, such an innovation requires upgrade of welding equipment [37].

Conclusions

The conducted studies on the formation of the USW lap-joints from the PEI adherends and the PEI-impregnated prepregs based on the CF-fabric without any EDs enabled to conclude the following. The more homogeneous macrostructure, the maintained structural integrity of both the CF-fabric in the prepregs and the joined PEI plates, as well as the maximum strength properties (tensile strength) were observed for the USW lap-joints with the minimum polymer content in the prepreg (at the PEI/CF-fabric ratio of 23/77). In this case, rising the USW duration from 400 up to 800 ms radically changed the macrostructure of the fusion zone, while the tensile strength did not vary significantly (σ = 42–48 MPa). This fact confirmed that the optimization of the USW parameters had to be based not only on a comparison of the σ_f values, the contribution of adhesive strength to which could not be decisive, but also on a detailed analysis of the structural characteristics.

The FEM-based theoretical investigations of the influence of the PEI/CF-fabric ratios in the prepregs on the deformation response of the USW lap-joints were carried out as well. The problem of the quantitative analysis was solved under the conditions of the macroscopic bending development, identifying the processes preceding the onset of fracture of the USW lap-joints. It was shown that the prepreg thicknesses and, accordingly, the PEI/CF ratios did not exert a noticeable effect on the strain–stress (tensile) diagrams, while the determining factor was the adhesion level. It was revealed that different adhesion levels in combination with the specified PEI properties the sample dimensions determined the fracture mechanism. In all considered cases, bending of the PEI adherends was observed, initiated at the edge of the USW lap-joints. It enhanced the development of plastic strains in this area when using the tensile testing scheme.

The analysis of the cross-sectional structure of the USW lap-joints showed their reliable macrostructure and the insufficient interlayer adhesion level at the optimal ratio of the prepreg components and the USW duration of 520 ms, determined using the RSM method.

It was shown that it is possible to form USW prepreg-joints characterized by the high LSS level at t = 750 ms and the PEI/CF-fabric ratio of 57/43. According to the authors, the reason was a significant difference in the nature of the transmission of ultrasonic vibrations through the PEI adherends 2 mm thick, in contrast to the thin (but of higher strength) prepreg, the basis of which was the reinforcing CF-fabric. The obtained results indicate that the USW technique has prospects for industrial manufacturing of laminates.

Acknowledgments

The work was performed according to the government research assignment for ISPMS SB RAS, project FWRW-2021-0010.

REFERENCES

[1] Gallego-Juárez, J. A. and Graff, K. F. (2015). Power Ultrasonics: Applications of High-Intensity Ultrasound, Elsevier, Amsterdam, pp. 295–312. DOI: 10.1016/B978-1-78242-028-6.00001-6.

[2] Tsiangou, E., de Freitas, S. T., Villegas, I. F., and Benedictus, R. (2019). Investigation on energy director-less ultrasonic welding of polyetherimide (PEI)-to epoxy-based composites. Composites Part B: Engineering, 173, pp. 107014. DOI: 10.1016/j.compositesb.2019.107014.

[3] Tolunay, M. N., Dawson, P. R., and Wang, K. K. (1983). Heating and bonding mechanisms in ultrasonic welding of thermoplastics. Polym. Eng. Sci. 23, 726–733. DOI: 10.1002/pen.760231307.

[4] Khatri, B., Roth, M. F., and Balle, F. (2022). Ultrasonic Welding of Additively Manufactured PEEK and Carbon-Fiber-Reinforced PEEK with Integrated Energy Directors. Journal of Manufacturing and Materials Processing, *7*(1), pp. 2. DOI: 10.3390/jmmp7010002.

[5] Suresh, K. S., Rani, M. R., Prakasan, K., Rudramoorthy, R. (2007). Modeling of temperature distribution in ultrasonic welding of thermoplastics for various joint designs. Journal of Materials Processing Technology, 186(1-3), pp.138-146.

[6] Villegas, I.F., Bersee, H.E.N. (2010). Ultrasonic welding of advanced thermoplastic composites: An investigation on energy-directing surfaces. Adv. Polym. T echnol., 29, pp.112–121.

[7] Wang, X., Yan, J., Li, R. and Yang, S. (2006). FEM Investigation of the Temperature Field of Energy Director During Ultrasonic Welding of PEEK Composites, Journal of Thermoplastic Composite Materials, 19, pp.593-607.

[8] Goto, K., Imai, K., Arai, M., Ishikawa, T. (2019). Shear and tensile joint strengths of carbon fiber-reinforced thermoplastics using ultrasonic welding. Compos. Part A Appl. Sci. Manuf., 116, pp.126–137.

[9] Villegas, I.F., Palardy, G. (2017). Ultrasonic welding of CF/PPS composites with integrated triangular energy directors: Melting, flow and weld strength development. Compos. Interfaces, 24, pp.515–528.

[10] Lionetto, F., Dell'Anna, R., Montagna, F., and Maffezzoli, A. (2016). Modeling of continuous ultrasonic impregnation and consolidation of thermoplastic matrix composites. Composites Part A: Applied Science and Manufacturing, 82, pp.119-129. DOI: 10.1016/j.compositesa.2015.12.004.

[11] Gomer, A., Zou, W., Grigat, N., Sackmann, J., and Schomburg, W. K. (2018). Fabrication of fiber reinforced plastics by ultrasonic welding. Journal of Composites Science, 2(3), pp. 56. DOI:10.3390/jcs2030056

[12] Yan, J. C., Wang, X. L., Li, R. Q., Xu, H. B., and Yang, S. Q. (2007). The effects of energy director shape on temperature field during ultrasonic welding of thermoplastic composites. Key Engineering Materials, 353, pp. 2007-2010. DOI: 10.4028/www.scientific.net/kem.353-358.2007.

[13] Palardy, G., Villegas, I.F. (2017) On the effect of flat energy directors thickness on heat generation during ultrasonic welding of thermoplastic composites. Compos. Interfaces, 24, pp. 203–214. DOI: 10.1080/09276440.2016.1199149.

[14] Bonmatin, M., Chabert, F., Bernhart, G., Cutard, T., and Djilali, T. (2022). Ultrasonic welding of CF/PEEK composites: Influence of welding parameters on interfacial temperature profiles and mechanical properties. Composites Part A: Applied Science and Manufacturing, 162, pp. 107074. DOI: 10.1016/j.compositesa.2022.107074.

[15] Tsiangou, E., Teixeira de Freitas, S., Villegas, I.F., Benedictus, R. (2020) Ultrasonic welding of epoxy- to polyetheretherketone - based composites: Investigation on the material of the energy director and the thickness of the coupling layer. J. Compos. Mater., 54, pp. 3081–3098. DOI: 10.1177/0021998320910207.

[16] Tao, W., Su, X., Wang, H., Zhang, Z., Li, H., Chen, J. (2019) Influence mechanism of welding time and energy director to the thermoplastic composite joints by ultrasonic welding. J. Manuf. Process., 37, pp.196–202. DOI: 10.1016/j.jmapro.2018.11.002.

[17] Wang, J., Lu, C., Xiao, C., Cheng, J., Ren, R., and Xiong, X. (2023). Heat distribution simulation and effects of ultrasonic welding amplitude on carbon fiber/polyetherimide composite joint properties. Materials Letters, 340, pp. 134148. DOI: 10.1016/j.matlet.2023.134148.

[18] Chuah, Y.K., Chien, L.H., Chang, B.C., Liu, S.J. (2000) Effects of the shape of the energy director on far-field ultrasonic welding of thermoplastics. Polym. Eng. Sci., 40, pp.157–167. DOI: 10.1002/pen.11149.

[19] Li, G., Zhao, J., Jiang, J., Jiang, H., Wu, W., and Tang, M. (2018). Ultrasonic strengthening improves tensile mechanical performance of fused deposition modeling 3D printing. The International Journal of Advanced Manufacturing Technology, 96, pp. 2747-2755. DOI: 10.1007/s00170-018-1789-0.

[20] Reis, J.P., de Moura, M., and Samborski, S. (2020) Thermoplastic composites and their promising applications in joining and repair composites structures: A review. Materials, 13, pp. 5832. DOI:10.3390/ma13245832.

[21] Korycki, A., Garnier, C., Bonmatin, M., Laurent, E., and Chabert, F. (2022). Assembling of Carbon Fibre/PEEK Composites: Comparison of Ultrasonic, Induction, and Transmission Laser Welding. Materials, 15(18), pp. 6365. DOI: 10.3390/ma15186365.

[22] Tsiangou E, Teixeira de Freitas S, Fernandez Villegas I and Benedictus R. (2019) Investigation on energy director-less ultrasonic welding of polyetherimide (PEI)- to epoxy-based composites. Compos. B Eng. 173, pp. 107014. DOI: 10.1016/j.compositesb.2019.107014.
[23] Chukov, D.I., Stepashkin, A.A., Gorshenkov, M.V., Tcherdyntsev, V.V., and Kaloshkin, S.D. (2014). Surface modification of carbon fibers and its effect on the fiber–matrix interaction of UHMWPE based composites. Journal of Alloys and Compounds, 586, pp. S459–S463. DOI: 10.1016/j.jallcom.2012.11.048.
[24] Alexenko, V.O., Panin, S.V., Stepanov, D.Y., Byakov, A.V., Bogdanov, A.A., Buslovich, D.G., Panin, K.S., and Tian, D. (2023) Ultrasonic Welding of PEEK Plates with CF Fabric Reinforcement—The Optimization of the Process by Neural Network Simulation. Materials, 16, pp. 2115. DOI: 10.3390/ma16052115.
[25] Villegas, Irene F., van Moorleghem, Regis (2018). Ultrasonic welding of carbon/epoxy and carbon/PEEK composites through a PEI thermoplastic coupling layer. Composites Part A: Applied Science and Manufacturing, 109, pp.75-83. DOI: 10.1016/j.compositesa.2018.02.022.
[26] Panin, S.V., Stepanov, D.Y. and Byakov, A.V. (2022) Optimizing Ultrasonic Welding Parameters for Multilayer Lap Joints of PEEK and Carbon Fibers by Neural Network Simulation. Materials, 15(19), pp. 6939. DOI: 10.3390/ma15196939.
[27] Ding, G., Feng, P., Wang, Y., and Ai, P. (2022). Novel pre-clamp lap joint for CFRP plates: Design and experimental study. Composite Structures, 302 (2), pp. 116240. DOI: 10.1016/j.compstruct.2022.116240.
[28] Oliveira, P. R., Virgen, G. P. G., Imbert, M., Beisel, S., May, M., Panzera, T. H., Hiermaier S. and Balle, F. (2023). Ultrasonically welded eco-friendly sandwich panels based on upcycled thermoplastic core: An eco-mechanical characterisation. Resources, Conservation & Recycling Advances, 20, pp. 200187. DOI: 10.1016/j.rcradv.2023.200187.
[29] Xiong, H., Hamila, N., and Boisse, P. (2019). Consolidation modeling during thermoforming of thermoplastic composite prepregs. Materials, 12(18), pp. 2853. DOI: 10.3390/ma12182853.
[30] Panin, S. V., Bochkareva, S. A., Panov, I. L., Alexenko, V. O., Byakov, A. V., and Lyukshin, B. A. (2023). Experimental and Numerical Studies on the Tensile Strength of Lap Joints of PEEK Plates and CF Fabric Prepregs Formed by Ultrasonic Welding. In Progress in Continuum Mechanics pp. 321-354. DOI: 10.1007/978-3-031-43736-6_19.
[31] Gunyaev, G. M. Structure and Properties of Polymeric Fibrous Composites. Moscow, Khimiya, 1981, 230 p. (in Russian).
[32] Altenbach, H., Altenbach, J., Kissing, W., and Altenbach, H. (2004). Mechanics of composite structural elements. Berlin: Springer-Verlag. pp. 122-297. DOI: 10.1007/978-3-662-08589-9.
[33] Skudra, A.M., Bulavs F.Ya. Strength of Reinforced Composites, Moscow, Khimiya, 1982, 216 p. (in Russian))
[34] Myers, R. H. (1999). Response surface methodology—current status and future directions. Journal of Quality Technology, 31(1), pp. 30-44. DOI: 10.1080/00224065.1999.11979891.
[35] Khuri AI. (2017) A general overview of response surface methodology. Biom Biostat Int J.,5(3), pp. 87-93. DOI: 10.15406/bbij.2017.05.00133.
[36] Kosmachev, P.V., Alexenko, V.O., Bochkareva, S.A., Panin, S.V. (2021) Deformation Behavior and Fracture Patterns of Laminated PEEK- and PI-Based Composites with Various Carbon-Fiber Reinforcement. Polymers, 13, pp. 2268. DOI: 10.3390/polym13142268.
[37] Jongbloed Bram, Teuwen Julie, Palardy Genevieve, Villegas Irene Fernandez, Benedictus Rinze (2020). Continuous ultrasonic welding of thermoplastic composites: Enhancing the weld uniformity by changing the energy director. J Compos Mater, 54 (15), pp. 2023-2035.